Available online at www.eccomasproceedia.org
Eccomas Proceedia COMPDYN (2023) 949-960

ECCOMAS
Proceedia

COMPDYN 2023
9th ECCOMAS Thematic Conference on
Computational Methods in Structural Dynamics and Earthquake Engineering
M. Papadrakakis, M. Fragiadakis (eds.)
Athens, Greece, 12-14 June 2023

# CONTINUOUS STRAIN FIELD ESTIMATION FOR CAST-IN-SITU REINFORCED CONCRETE SANDWICH WALLS UNDER CYCLIC LATERAL IN-PLANE LOADING

**Carlos Andrés Riascos González[1], Paolino Cassese[1], Antonio Occhiuzzi[1,2] and Carlo Rainieri[1]**

[1] National Research Council (CNR), Construction Technologies Institute (ITC)
c/o Polo Tecnologico di San Giovanni a Teduccio, Corso Nicolangelo Protopisani, Naples, Italy
cassese@itc.cnr.it, riascos@itc.cnr.it, rainieri@itc.cnr.it, occhiuzzi@itc.cnr.it,

[2] University Parthenope, Department of Engineering
Centro Direzionale Isola C4, 80143 Naples, Italy
antonio.occhiuzzi@uniparthenope.it

## Abstract

*Cast-in-situ reinforced concrete sandwich walls represent a promising solution for energy-efficient housing. Nevertheless, their use in earthquake-prone areas is fairly limited because of the lack of seismic guidelines. Furthermore, the evaluation of seismic response of such a structural typology can be partially considered a still open issue. In this study, the in-plane seismic behavior of cast-in-situ reinforced concrete sandwich walls is investigated through cyclic experimental tests on real scale sandwich walls composed of a central layer of insulating material closed between two external reinforced shotcrete layers. Experimental load-displacement curves and observed damage are briefly described. A special focus on the deformative mechanisms of the walls is dealt with. A hybrid experimental-numerical procedure is proposed,to derive continuous strain fields starting from local discrete experimental measures, with promising preliminary results.*

**Keywords:** Full scale Cyclic Experimental Tests, Seismic Performance, Sandwich Walls, Radial Basis Function, Strain Fields.

ISSN:2623-3347 
Peer-review under responsibility of the organizing committee of COMPDYN 2023.
doi: 10.7712/120123.10448.20710

# 1 INTRODUCTION

Sandwich Panels (SP) are intended as structural or non-structural elements characterized by at least two layers made of high strength material, called "wythes", divided each other by at least one layer of material with lower strength (named "core") [1]. SPs are commonly adopted in civil construction sector since 1950 as non-structural prefabricated members, due to their great versatility and the possibility to achieve high performance by properly combining the constituent materials ([2]-[3]). In the last decades, SPs have been also used as structural solution for civil buildings in areas with moderate seismicity and many technological systems have been developed and applied on field with increased success ([4]-[8]). Very recently, some studies proposed to use SPs in seismic and energy integrated retrofit of buildings [7].

In addition to the most common and widespread prefabricated version of SPs, cast-in-situ (or sprayed-in-situ) approach is becoming more attractive since it allows to solve relevant construction issues related to transportation and erection of panels, and several research studies are available in literature in this line ([9]-[11]). Despite the considerable interest concerning cast-in-situ Reinforced Concrete Sandwich Panels (cRCSPs), so far, no seismic design guideline is available and, moreover, limited research studies focused to a detailed assessment of the in-plane cyclic response can be found in literature, thus someway limiting their potential [12].

Basically, cRCSP-based walls, i.e., horizontal elements made of a series of sandwiched modules, behave almost like ordinary lightly RC walls, therefore their response is mostly governed by a flexure-shear interaction, whose features are mainly associated with structural variables such as: dimensions, presence of openings, boundary conditions, and axial load level [13]. Determining the actual deformative mechanisms due to flexure or shear during experimental tests on RC large-scale members may represent a crucial point towards a complete understanding of the mechanical response as well as a reliable validation of numerical modelling results. Such an objective is often challenging, especially for (i) large specimens like real-scale walls and (ii) low load levels. Furthermore, only discrete measures in several points of the specimens may be derived [14]. On the other hand, commonly, Finite Element Method (FEM) plane models are used to reproduce the experimental behavior of cRCSP-based walls ([15], [16]). As known, those models are able to return the numerical point-by-point response of the wall, that cannot be directly compared with the corresponding experimental results, therefore force-displacement curves, cracking patterns, and limited local measurements are used to the scope. Recently, the use of advanced non-contact measurement techniques, such as Digital Image Correlation (DIC), is gaining popularity in order to reduce this gap, even if in the case of large-scale experimental tests some issues need to be improved and satisfying results can be obtained only for limited portions of the specimen [17].

The literature describes a chronological interval of approximately five decades between the intensified use of mesh-based methods, such as Finite Difference Method (FDM) and Finite Element Method (FEM), and the relatively recent rise of numerical techniques based on Radial Basis Function (RBF) [18]. The growth of this technique is based on its great capacity to work with: irregular geometries, moving boundaries, higher dimensional problems, and to dispense with conventional meshing issues [19]. Therefore, RBF-based methods have been applied to solve computational fluid dynamics computations, flows simulations with a moving boundary (e.g., bridges, aircrafts, and wind turbines) and bioengineering problems [20]. Among those methods, the following ones stand out: the RBF collocation method (RBFCM) [21], the Hermite collocation method [22], the integrated RBF method [23], the localized RBF method [24] and the method of particular solutions [25]. Currently, very few and preliminary studies concerning the use of RBF-based methods for civil engineering applications are available in the literature. One of the most recent and interesting of those is reported in [26], wherein the Authors solved

the ideal case of a composite wall, made of two different elastic materials, under different simple loading conditions.

The present study aims at contributing to investigate the resisting mechanisms of cRCSP walls under combined in-plane lateral cyclic displacement and constant vertical load. To achieve the objective, (i) two experimental tests on squat full-scale cRCSP walls were carried out and (ii) a new hybrid experimental-numerical procedure to obtain continuous strain fields was developed and preliminary applied to fit experimental data. In the following, the experimental campaign and the main outcomes are briefly described in Section 2, whilst methodology and preliminary results of the proposed procedure are discussed in Section 3. Finally, some relevant conclusions and future developments are outlined in Section 4.

## 2 EXPERIMENTAL CAMPAIGN AND OUTCOMES

### 2.1 Specimens, procedure and measuring system

An extensive description of the experimental program is reported in [27]. The cRCSPs considered in this study were composed by two external layers of reinforced sprayed concrete and a central layer of Sintered Expanded polystyrene (EPS). The mean value of concrete cylindrical compressive strength was 26 MPa. Steel reinforcement with 2.5 mm diameter and 5 cm square mesh was used, characterized by tensile strength of 700 MPa. These panels, named W1 and W2, had the same in-plane rectangular shape, with length and height equal to 400 cm and 300 cm, respectively. Each of the two external wythes had a nominal thickness of 4 cm, and whilst the EPS core had a thickness of 10 cm for a total element thickness equal to 18 cm.

Test procedure consisted of a first phase during which the specimens were exposed to vertical axial load, equal to 50 kN and 100 kN respectively for W1 and W2. Later, a cyclic in-plane horizontal displacement protocol was applied at the top of the specimens. Such a protocol involved nine sets, each one involving three internal cycles at the same amplitude. The applied Inter-story Drift Ratios (IDR), namely the ratio of the maximum horizontal displacement applied during the steps to the height of the panels, were: 0.1, 0.2, 0.4, 0.6, 0.75, 1.0, 1.25, 1.5 and 2.0 (%).

In order to investigate in detail, the deformative mechanisms acting within the walls during the tests, the specimens were instrumented with 12 Linear Vertical Displacement Transducers (LVDTs) that allowed deriving the variation of length associated with discrete segments, as evidenced with red lines in Figure 1. Additional transducers were used to monitor the occurrence of sliding between the panel and the lower or upper boundary beams.

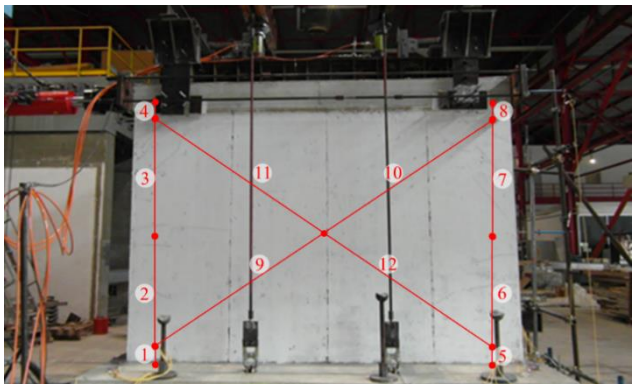


Figure 1: Schematic distribution of displacement transducers.

## 2.2 Global response and deformability contributions

Figure 2 illustrates the global experimental response of both specimens in terms of force versus displacement hysteretic curves. The geometrical symmetry of the walls can be substantially found in the symmetry of the response both in push (-) and pull (+) directions, at least up to the peak condition, beyond which slightly different damage evolution were observed up to the collapse. By computing the initial stiffness values as the ratio of the average force and the average displacement corresponding to the peak of the first set (IDR=0.1%), the values 67.5 kN/mm and 71.3 kN/mm, are obtained for W1 and W2, respectively. In the second set, a non-linear considerable reduction in the stiffness of the elements is observed on the backbone curve, confirming that in this set the reinforcing elements are approaching their yield stress. During the third set, both the specimens reach their shear strength for an IDR value almost equal to 0.4%. Specifically, specimen W1 reached a peak value of 308.1 kN, averaged between push and pull, whereas a slightly higher value was achieved by specimen W2. Beyond this set, the softening phase took place until the failure was approached, this latter conventionally established as corresponding to 15% reduction of the recorded shear load with respect to the maximum value. Both specimens were interested by ductile failure mode.

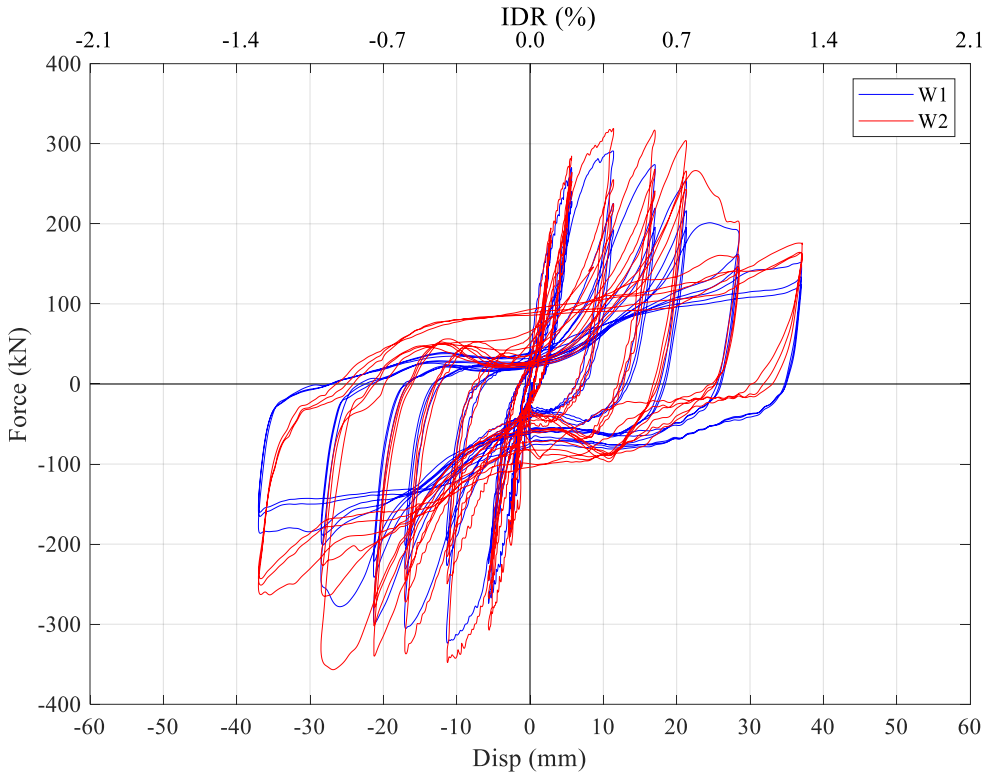


Figure 2: Mechanical response of specimens W1 and W2.

Figure 3 shows the final damage patterns observed for specimens W1 and W2, respectively. At both the bottom corners, concrete appeared completely crushed. Most of the cracks took place within the bottom half of the specimens, and they started at the lateral edges as horizontal and rapidly evolved along diagonal direction with increasing angle of inclination towards the wall center.

Definitely, specimens W1 and W2 showed a fairly similar mechanical response. Therefore, in the following, specimen W1 was considered as control case.

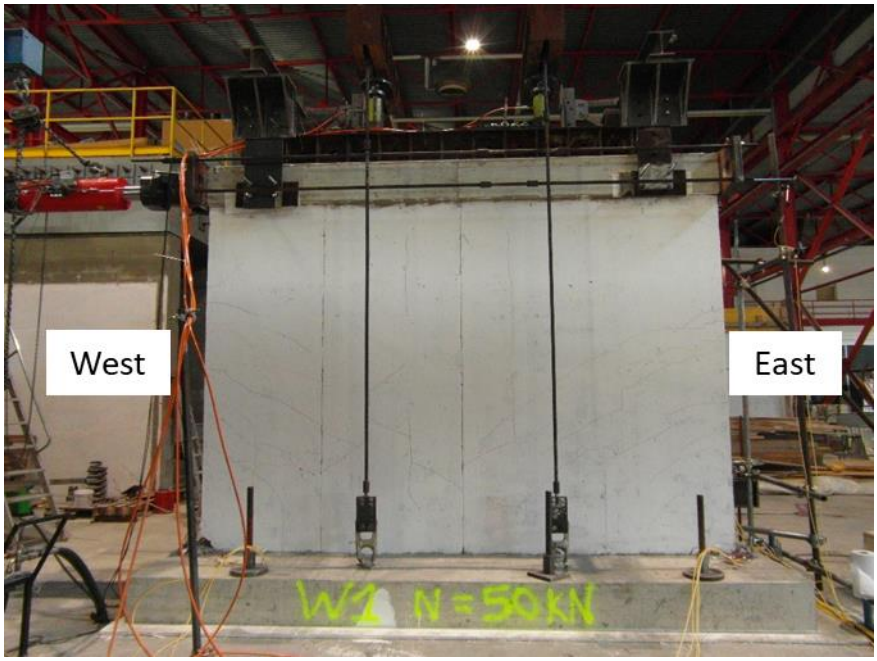


(a)

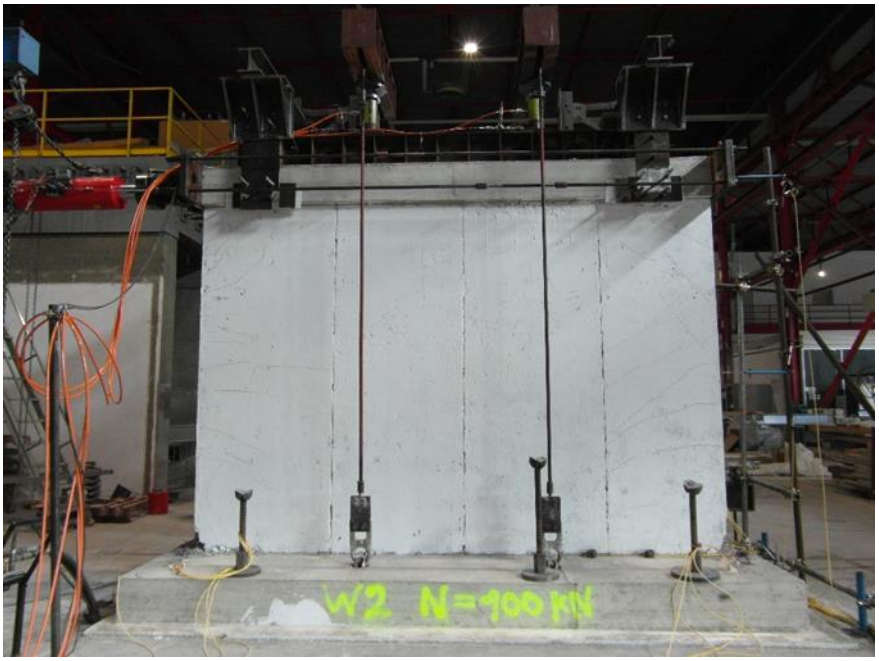


(b)

Figure 3: Final observed damage patterns for specimens W1 and W2.

## 3 CONTINUOUS STRAIN FIELDS

### 3.1 Methodology

The applied methodology is schematically illustrated in Figure 4. The starting point is given by the considered experimental problem, which in the present study consists of testing cRCSP walls under combined axial and horizontal loads. Such a condition can be expressed by means

of an analytical representation, called Boundary Value Problem (BVP) [26], as the core of the realization, which naturally has a set of boundary conditions. However, the experimental problem is characterized by several measurements that capture the actual behavior of the specimen in question, which is assigned to a group called "alternative measurements". These data enrich the information available for the associated BVP, as well as allow establishing some particularities in the boundary conditions. Therefore, a hybrid (H-) RBFCM is adopted herein that uses all the available information, with both analytical and experimental provenance, to develop a digital model of the experimental test. Once this representation is obtained, the H-RBFCM provides a continuously distributed hybrid solution that is not available in conventional methods, these latter based exclusively on FEM models or directly in the post-processing of the experimental results. In the case of the present experimental problem, concerning the test W1 described in the section 2, the H-RBFCM outputs are represented by the cRCSP displacement fields, from which continuous strain fields over the entire domain can be evaluated.

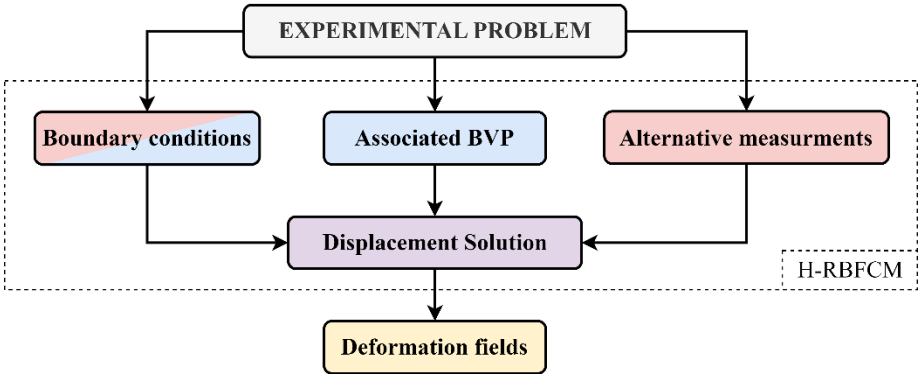


Figure 4: H-RBFCM procedure flowchart.

It is important to note that there are several types of RBFs, among which linear (LI), logarithmic (LO), Gaussian (GA), multiquadric (MQ) stand out ([28], [29]). In this study, a MQ type RBF was used, which was proposed as a revolutionary solution in topographic applications in 1971 [30]. A generalized expression of the RBF-MQ is given in Eq. (1).

$$\phi(R) = (R^2 + c^2)^{n-3/2} \tag{1}$$

Where $R = \left\|\vec{r} - \vec{p}_j\right\|$ indicates the Euclidean distance between an arbitrary point $\vec{r}$ and the j-th position point $\vec{p}_j$ or center, where the features of the continuous field is known. On the other hand, $c$ represents the shape parameter, which has a strong influence on the accuracy and stability of the RBFs approximation [31]. Some formulations have been proposed in literature to determine an optimal value of $c$, usually as a function of: (i) the number of centers (N), (ii) the diameter D of the smallest imaginary circle that encompasses all the centers, and (iii) the distance $d_i$ from the i-th center to the nearest neighbor. Among the most commonly used formulations, within the present methodology the one developed by Franke [19] is used ($c = 1.25D/\sqrt{N}$). However, there are currently several optimization methods available, such as Leave-One-Out Cross Validation (LOOCV), Residue-Error Cross Validation (RECV) and Modified Knot Insertion (MKI) [32].

For the realization of the BVPs, each dependent variable can be represented as a continuous function, $s(\vec{r})$, as shown in Eq. (2). In this equation: $a_j$ is the coefficient of the j-th analytical center, $N_s$ is the number of analytical centers, $\tilde{a}_k$ is the coefficient of the k-th experimental center, and $N_e$ is the number of experimental centers. Thus, the model has a total number of centers

equal to $N = N_s + N_e$. In addition, the participation of a n-degree polynomial $P(\vec{r})$ was included to facilitate reaching the boundary conditions. Substituting the expressions of the dependent variables in the BVP, the coefficients can be determined through the least-squares method as detailed in [20].

$$s(\vec{r}) \approx P_n(\vec{r}) + \sum_{j=1}^{N_s} a_j \phi\left(\left\|\vec{r} - \vec{p}_j\right\|\right) + \sum_{k=1}^{N_e} \tilde{a}_k \phi\left(\left\|\vec{r} - \vec{q}_k\right\|\right) \tag{2}$$

Eq. (3) reports the strong formulation of a generic BVP.

$$\begin{aligned} \boldsymbol{\mathcal{L}}\, \boldsymbol{w}(x,y) &= \boldsymbol{f}(x,y), \quad \vee \quad (x,y) \;\epsilon\; \boldsymbol{\Omega} \\ \boldsymbol{\mathcal{B}}^h\, \boldsymbol{w}(x,y) &= \boldsymbol{h}(x,y), \quad \vee \quad (x,y) \;\epsilon\; \partial\boldsymbol{\Omega}^h \\ \boldsymbol{\mathcal{B}}^{\mathrm{g}}\, \boldsymbol{w}(x,y) &= \mathbf{g}(x,y), \quad \vee \quad (x,y) \;\epsilon\; \partial\boldsymbol{\Omega}^{\mathrm{g}} \end{aligned} \tag{3}$$

In Eq. (3), $\boldsymbol{\mathcal{L}}$ is the differential operator containing the mechanical formulation of strain elastic plane problem, whilst $\boldsymbol{\Omega}$ represents the domain, and $\partial\boldsymbol{\Omega}^h$ and $\partial\boldsymbol{\Omega}^{\mathrm{g}}$ constitute the Newmann and Dirichlet boundary conditions, respectively. The horizontal and vertical displacement fields are described by the dependent functions $u(x,y)$ and $v(x,y)$, correspondingly. Both expressions constitute the tensor $\boldsymbol{w}(x,y)$, as defined in Eq. (4). The operator $\boldsymbol{\mathcal{L}}$ is described in Eq. (5), and the operator defining the Neumann-type boundary conditions ($\boldsymbol{\mathcal{B}}^h$) is represented in Eq. (6). The coefficients λ and μ, reported in Eqs. (5) and (6), are the Lamé's constants ([26], [28]), as specified in Eq. (7). Additionally, the Dirichlet-type conditions ($\boldsymbol{\mathcal{B}}^{\mathrm{g}}$) in this problem are defined as the identity matrix with compatible dimensions with respect to the problem formulation.

$$\boldsymbol{w}(x,y) = [u(x,y) \quad v(x,y)]^T \tag{4}$$

$$\boldsymbol{\mathcal{L}} = \begin{bmatrix} (\lambda+2\mu)\dfrac{\partial^2}{\partial x^2} + \mu\dfrac{\partial^2}{\partial y^2} & (\lambda+\mu)\dfrac{\partial^2}{\partial x \partial y} \\ (\lambda+\mu)\dfrac{\partial^2}{\partial x \partial y} & (\lambda+2\mu)\dfrac{\partial^2}{\partial y^2} + \mu\dfrac{\partial^2}{\partial x^2} \end{bmatrix} \tag{5}$$

$$\boldsymbol{\mathcal{B}}^h = \begin{bmatrix} (\lambda+2\mu)\dfrac{\partial}{\partial x} + \mu\dfrac{\partial}{\partial y} & \lambda\dfrac{\partial}{\partial y} + \mu\dfrac{\partial}{\partial x} \\ \lambda\dfrac{\partial}{\partial x} + \mu\dfrac{\partial}{\partial y} & (\lambda+2\mu)\dfrac{\partial}{\partial y} + \mu\dfrac{\partial}{\partial x} \end{bmatrix} \tag{6}$$

$$\lambda = \frac{E\nu}{(1+\nu)(1-2\nu)}; \qquad \mu = \frac{E}{2(1+\nu)} \tag{7}$$

The response of the tested specimens can be completely defined by identifying the horizontal displacement at the top edge, $\delta_x$, as shown in Figure 5(a). In this way, the element boundaries may be divided into the 4 edges, $\partial\Omega_i$ , $i = 1, \ldots, 4$, as shown in Figure 5 (b). These boundaries can be grouped as follows:

- $\partial\Omega_1 \cup \partial\Omega_3 \;\epsilon\; \partial\boldsymbol{\Omega}^h$;

- $\partial\Omega_2$ and $\partial\Omega_4$ compose the group of boundaries described by the Dirichlet formulation, where $\partial\Omega_2$ integrates the horizontal displacement $\delta_x$ and the vertical displacement function $f_y(x)$;
- $\partial\Omega_4$ states that the element remains stationary at the base.

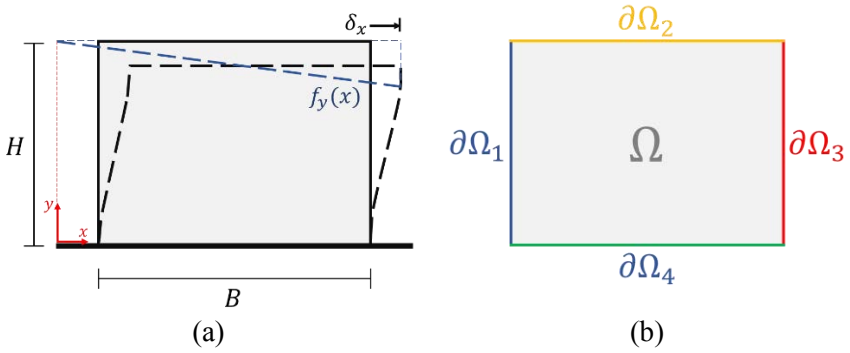


Figure 5: Associated BVP representation: (a) deformed scheme (b) boundaries.

Due to the high upper beam stiffness of the cRCSP, $f_y(x)$ is described as a linear function. In this way, the known deformations of the analytical centers are denoted as $u_a$ and $v_a$ along horizontal and vertical directions, respectively, whilst that of the experimental centers are indicated as $u_e$ and $v_e$.

### 3.2 Application

The RBF-MQ was employed in this study with $n = 2$, see Eq. (1). In addition, the modulus of elasticity was estimated as $E_c = 4700\sqrt{f'_c}$ in MPa and a Poisson's ratio $\nu = 0.2$ was assumed. For the control specimen (W1), the coordinates of the points were evaluated during the first cycle of the first loading set of the displacement protocol, in pull direction, in order to evaluate the capacity of the methodology to identify the presence of some damage, relatively low, in the cRCSPs.

To calculate the deformations of the experimental centers, and to configure the boundary condition $\partial\Omega_2$, it is necessary to use the data captured by the LVDTs network. For this purpose, it has been employed the configuration shown in Figure 6.

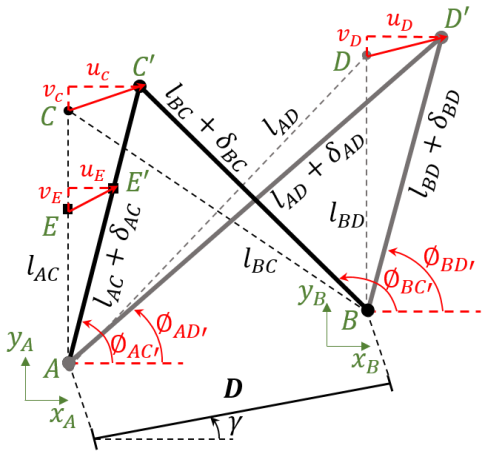


Figure 6: LVDTs deformation diagram.

This diagram shows the configuration of four measurement lines, which can be composed of a single LVDT or by LVDTs arranged in series. These lines form two triangles whose base arises from joining points A and B, which are separated by a distance D. In the original configuration these triangles have vertices ABC and ABD, while in their deformed position they arise from vertices ABC' and ABD', respectively. The lengths of the four lines are denoted as $l_{AC}$, $l_{AD}$, $l_{BC}$ and $l_{BD}$ and the deformations presented in each of them as $\delta_{AC}$, $\delta_{AD}$, $\delta_{BC}$ and $\delta_{BD}$. Since all the sides of both triangles are known, the angles of each of the lines can be determined with the Eq. (8), where $\gamma$ is the slope of the segment joining points A and B. This formulation allows knowing the position of points C' and D' both in the horizontal direction and in the vertical direction. Additionally, for lines that have intermediate points, such as point E, their deformation components are also determined once the elongation of each line and its angle of inclination are known. In this sense, the deformation $u_e$ and $v_e$ are determined from the decomposition in the cartesian axes.

$$
\begin{aligned}
(l_{BC}+\delta_{BC})^2 &= (l_{AC}+\delta_{AC})^2 + D^2 + 2D(l_{AC}+\delta_{AC})cos(\theta_{AC}-\gamma) \\
(l_{BD}+\delta_{BD})^2 &= (l_{AD}+\delta_{AD})^2 + D^2 + 2D(l_{AD}+\delta_{AD})cos(\theta_{AD}-\gamma) \\
(l_{AC}+\delta_{AC})^2 &= (l_{BC}+\delta_{BC})^2 + D^2 + 2D(l_{BC}+\delta_{BC})cos(\pi-\theta_{BC}+\gamma) \\
(l_{AD}+\delta_{AD})^2 &= (l_{BD}+\delta_{BD})^2 + D^2 + 2D(l_{BD}+\delta_{BD})cos(\pi-\theta_{BD}+\gamma)
\end{aligned}
\tag{8}
$$

By combining the experimental information with that from the associated BVP and solving Eq. (3) using the least squares method, as established by [26], the coefficients $a_j$ and $\tilde{a}_k$ describing the coupled behavior of the panel in the horizontal and vertical direction are found. Once both displacement fields were obtained, the vertical strain field of each of the panels was calculated as derivative.

Figure 7 shows the continuous strain fields determined for the control specimens W1. In such a picture, the cracks observed during the first loading step on the specimens are also plotted as black bold lines.

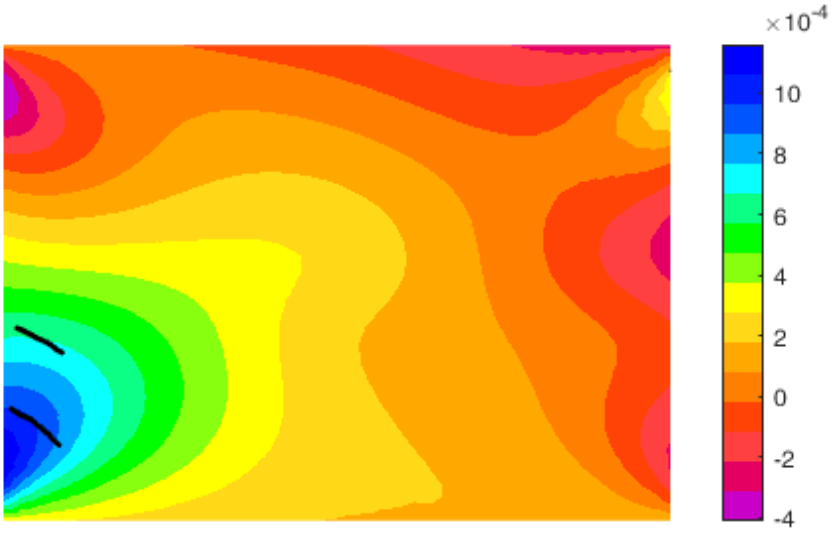


Figure 7: Comparison between H-RBFCM vertical strain and observed damage at first set: (a) W1 and (b) W2.

By analyzing the results, it can be noticed that the proposed H-RBFCM methodology was able to catch with reasonable approximation the region of the wall in which the presence of cracks was experimentally observed. On the other hand, the color map gives some helpful insight about the strain field of the panel, and, in such a way, tensile and compressive zones of the panel and regions of strain concentration may be identified and eventually used as comparison with the results of pure numerical solutions. Nevertheless, further research is needed to ensure full compatibility of strain fields at the boundaries and with cracking development at various stages of loading.

## 4. CONCLUSIONS AND FUTURE DEVELOPMENTS

In the present study, two experimental tests on squat full-scale cRCSP walls under in-plane cyclic and axial load were carried out. Two different levels of axial load were considered, one for each test, keeping constant the wall type. An instrumentation system made of 12 LVDTs was arranged to evaluate the deformative state of the walls during the tests. Main global experimental outcomes are:

- Specimens exhibited a symmetrical behavior characterized by high flexure-shear interaction, as confirmed by the final cracking patterns.
- Ductile failure mode was observed for both the tests.

The experimental assessment of the actual deformative mechanisms acting within cRCSP walls during the tests represents a relevant opportunity to improve the knowledge of their seismic response, although quite challenging. Such an issue has been investigated in this work and a new hybrid experimental-numerical procedure has been proposed, based on Radial Basis Function collocation method. The procedure was specified for the experimental case study and properly modified in order to use the punctual measures derived from the installed LVDTs as given boundary information. A very preliminary application has been carried out, considering the first loading set. The continuous strain fields have been derived for a control specimen and the comparison of the obtained results with the observed damage are promising. Future activities, currently under development, will explore (i) the use of different shape parameters, (ii) the comparison of H-RBFCM results with conventional FEM analysis, and (iii) the extension of the methodology to strongly non-linear response.

## REFERENCES

[1] E. Hamed, Modeling, analysis, and behavior of load-carrying precast concrete sandwich panels. *Journal of Structural Engineering*, **142**(7), 4016036, 2016.

[2] J. M. Davies, *Lightweight sandwich construction*. John Wiley & Sons, 2008.

[3] A. Ahmad, Y. Singh, In-plane behaviour of expanded polystyrene core reinforced concrete sandwich panels. *Construction and Building Materials*, 269, 121804, 2021.

[4] T. D. Bush, G. L. Stine, Flexural behavior of composite precast concrete sandwich panels with continuous truss connectors. *PCI Journal*, **39**(2), 112–121, 1994.

[5] A. Benayoune, A. A. A. Samad, D. N. Trikha, A. A. A. Ali, A. M. Akhand, Precast reinforced concrete sandwich panel as an industrialised building system. *International Conference on Concrete Engineering and Technology University Malaya*, 2004.

[6] E. D. Losch, P. W. Hynes, R. Andrews Jr, R. Browning, P. Cardone, R. Devalapura, R. Donahey, S. Freedman, H. A. Gleich, G. Goettsche. State of the art of precast/prestressed concrete sandwich wall panels. *PCI Journal*, *56*(2), 131–176, 2011.

[7] N. Ademovic, A. Formisano, L. Penazzato, D. V. Oliveira, Seismic and energy integrated retrofit of buildings: A critical review. *Frontiers in Built Environment*, 8, 963337, 2022.

[8] A. Ahmad, Y. Singh, Flexural behavior of Expanded Polystyrene core Reinforced Concrete Sandwich Panels with different construction methods and end conditions. *Structures*, *34*, 2900–2911, 2021.

[9] A. Pavese, D. A. Bournas, Experimental assessment of the seismic performance of a prefabricated concrete structural wall system. *Engineering Structures*, **33**(6), 2049–2062, 2011.

[10] I. Ricci, M. Palermo, G. Gasparini, S. Silvestri, T. Trombetti. Results of pseudo-static tests with cyclic horizontal load on cast in situ sandwich squat concrete walls. *Engineering Structures*, **54**, 131–149, 2013.

[11] Refaei, F. A. I., El-Mihilmy, M. T., & Bahaa, T. M. (2015). Seismic behavior of sandwich panel walls. *World Applied Sciences Journal*, **33**(11), 1718–1731.

[12] P. Cassese, A. Bilotta, A. Bonati, A. Occhiuzzi, E. Cosenza, Seismic Performances of Reinforced Concrete Sandwich Walls, *Proceedings of Italian Concrete Days 2020*, (in print).

[13] E. Brunesi, R. Nascimbene, A. Pavese, Mechanical model for seismic response assessment of lightly reinforced concrete walls. *Earthquakes and Structures*, **11**(3), 461-481, 2016.

[14] P. Cassese, M. T. De Risi, G. M. Verderame, A modelling approach for existing shear-critical RC bridge piers with hollow rectangular cross section under lateral loads. *Bulletin of Earthquake Engineering*, **17**, 237-270, 2019.

[15] M. Palermo, T. Trombetti, Experimentally-validated modelling of thin RC sandwich walls subjected to seismic loads. *Engineering Structures*, **119**, 95-109, 2016.

[16] M. Serpilli, F. Clementi, S. Lenci, An experimental and numerical study on the in-plane axial and shear behavior of sprayed in-situ concrete sandwich panels. *Engineering Structures*, **232**, 111814 2021.

[17] B. Gencturk, K. Hossain, A. Kapadia, E. Labib, Y. L. Mo, Use of digital image correlation technique in full-scale testing of prestressed concrete structures. *Measurement*, **47**, 505-515, 2014.

[18] J. Lin, Y. Zhao, D. Watson, C. S. Chen, The radial basis function differential quadrature method with ghost points. *Mathematics and Computers in Simulation*, **173**, 105–114, 2020.

[19] I. Karakan, D. Gürkan, P. Avcı, A Comparison Between Meshless Radial Basis Function Collocation Method and Finite Element Method for Solving Poisson and Stokes Problems. *ArXiv, 2020, 14218*.

[20] C. Xie, S. Jia, Y. Li, C. An, C. Yang, Mapping Based Quality Metrics for Mesh Deformation Algorithms Using Radial Basis Functions. *Applied Sciences*, **11**(1), 59, 2020.

[21] E. J. Kansa, Multiquadrics—A scattered data approximation scheme with applications to computational fluid-dynamics—II solutions to parabolic, hyperbolic and elliptic partial differential equations. *Computers & Mathematics with Applications*, **19**(8–9), 147–161, 1990.

[22] G. E. Fasshauer, Solving partial differential equations by collocation with radial basis functions. *Proceedings of Chamonix*, *1997*, 1–8, 1997.

[23] D. Ngo-Cong, C. D. Tran, N. Mai-Duy, T. Tran-Cong, Incompressible smoothed particle hydrodynamics-moving IRBFN method for viscous flow problems. *Engineering Analysis with Boundary Elements*, **59**, 172–186, 2015.

[24] H. Zheng, Z. Yang, C. Zhang, M. Tyrer, A local radial basis function collocation method for band structure computation of phononic crystals with scatterers of arbitrary geometry. *Applied Mathematical Modelling*, **60**, 447–459, 2018.

[25] C. S. Chen, C. M. Fan, P. H. Wen, The method of approximate particular solutions for solving certain partial differential equations. *Numerical Methods for Partial Differential Equations*, **28**(2), 506–522, 2012.

[26] J. Xiong, J. Wen, H. Zheng, An improved local radial basis function collocation method based on the domain decomposition for composite wall. *Engineering Analysis with Boundary Elements*, *120*, 246–25, 2020.

[27] P. Cassese, C. Riascos, C. Rainieri, G. De Luca, A. Pavese, and A. Bonati, "Experimental study on the in-plane response of cast-in-situ reinforced concrete sandwich walls under combined vertical and horizontal load," *Procedia Struct. Integr.*, **44**, 774–781, 2023.

[28] H. Y. Hu, J. S. Chen, and W. Hu, "Weighted radial basis collocation method for boundary value problems," *Int. J. Numer. Methods Eng*., **69**(13), 2736–2757, 2007.

[29] D. Sturgill, *Variable shape parameter strategies in radial basis function methods*, PhD Thesis, 2009.

[30] R. L. Hardy, Theory and applications of the multiquadric-biharmonic method 20 years of discovery 1968–1988, *Comput. Math. with Appl.*, **19** (8–9), 163–208, 1990.

[31] L. Wang, Radial basis functions methods for boundary value problems: Performance comparison, *Eng. Anal. Bound. Elem.*, **84**, 191–205, 2017.

[32] L.H. Kuo, *On the selection of a good shape parameter for RBF approximation and its application for solving PDEs*. The University of Southern Mississippi, PhD Thesis, 2015.